THE LARGE VARIABLE MAGNETIC FIELD OF HD 126515 AND ITS IMPLICATIONS FOR THE RIGID-ROTATOR MODEL OF MAGNETIC STARS

GEORGE W. PRESTON
Hale Observatories, Carnegie Institution of Washington,
California Institute of Technology
Received 1969 December 16

ABSTRACT

The mean surface field H_s of the Sr-Cr-Eu star HD 126515 varies approximately sinusoidally between 10 and 17 kilogauss in a period of 130^d0. The effective field H_e oscillates between -2 and $+2$ kilogauss with a single wave in the same period. From the point of view of the rigid-rotator model, these results require that the star have a hemispherically asymmetric magnetic field, the principal features of which are represented by a dipole displaced from the center of the star in the direction opposite to its moment by 0.36 stellar radii. HD 126515 is also a spectrum variable, and the phase relations between the line intensity and H_s variations indicate in a general way that the heavy elements are concentrated in regions where the surface field is strongest.

I. INTRODUCTION

Following the discovery of resolved Zeeman patterns in the spectra of 53 Cam (Preston 1969a) and β CrB (Preston 1969b), the writer's attention was drawn to HD 126515 by Babcock's (1958) remarks that "profiles of some of the broader lines are unusual, showing in some cases a multiple structure." Examination of Babcock's spectrograms showed immediately that these multiple structures are partially or completely resolved Zeeman patterns and that the widths of these patterns vary considerably from plate to plate. These conclusions are readily apparent from inspection of the doublet and triplet patterns reproduced from two spectrograms in Figure 1 (Plate 3). The discussion that follows is based on twenty spectrograms (dispersion ~ 4.5 Å mm^{-1}), ten obtained by Babcock and ten obtained more recently by the writer with the coudé spectrographs of the 100-inch and 200-inch telescopes. A journal of all the observations is given in Table 1.

All unblended lines that show resolved Zeeman structure in HD 126515 in the spectral region λλ 4020–4620 are listed in Table 2, together with the measured Zeeman displacements for four spectrograms on which most of the patterns are resolved. The theoretical patterns for LS coupling are also given. All but six of the forty-three lines are doublets produced by $J \rightarrow J$ transitions for which the outermost π-components are the most intense. Five favorable triplet patterns and one quartet, Fe II λ4273.32, are also resolved. The longward σ-component of the weak triplet Fe I λ4210.35 cannot be measured because of an interfering blend. An apparent triplet pattern at λ4215.6 is actually the resultant of overlapping doublet patterns due to Sr II λ4215.52 and Cr II λ4215.77. The intensity-weighted mean displacements of the theoretical patterns in Lorentz units, z', are also given in Table 2. For the doublets, the z'-values differ from the z-values used by Babcock in that they refer to the centroids of the combined π and σ groups that are measured on the spectrograms.

The correlation between Δs_c and z' (or z for triplets) for spectrogram Pb 11155 shown in Figure 2 demonstrates clearly that the observed multiple structures are manifestations of the Zeeman effect. The slope of the least-squares line through the data points for all lines and the origin gives a field of $H_s = 16100 \pm 200$ (p.e.), according to equation
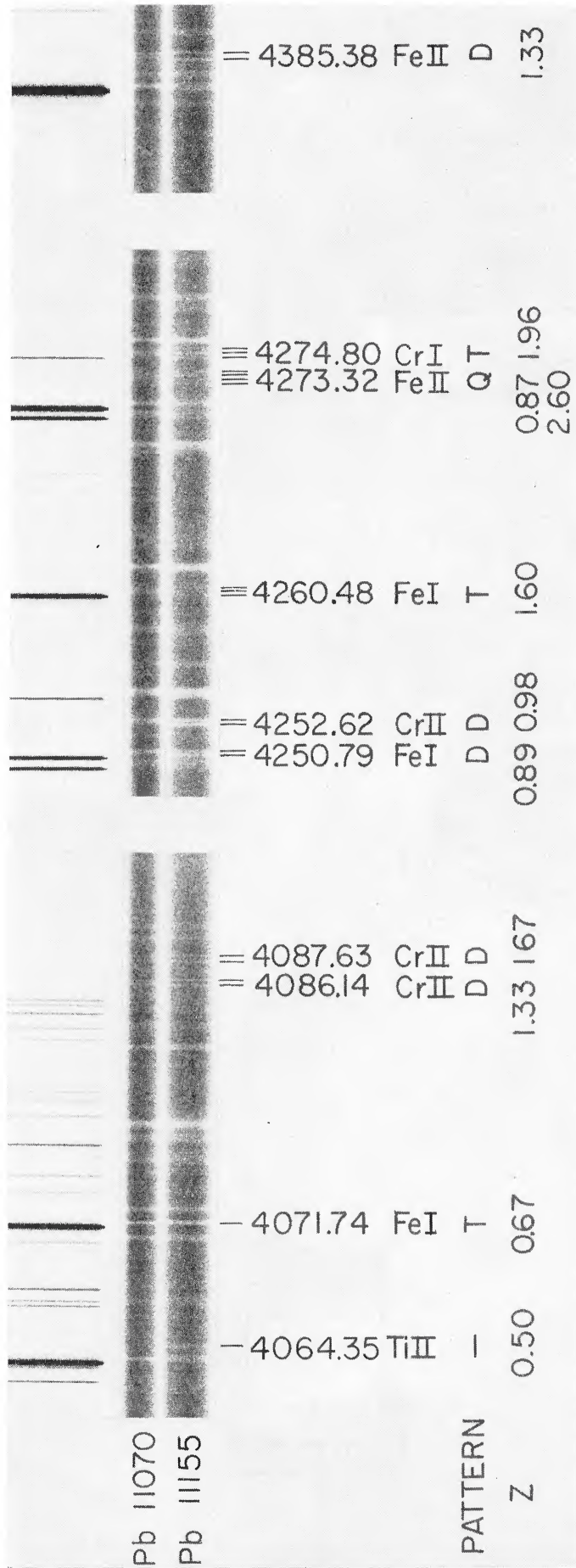
1059

PLATE 3

FIG. 1.—Reproductions of portions of two spectrograms of HD 126515 at phases 0.57 (Pb 11070) and 0.08 (Pb 11155). Zeeman doublets, triplets, and one quartet due to Fe II λ4273.32 are resolved at phase 0.08 when the mean surface field is 16000 gauss. At phase 0.57, $H_s \approx 10000$; only the most favorable doublets such as Cr II λ4086.14 and Fe II λ4385.38 are resolved. Note the sharpness of Fe I λ4071.74, which has the narrow pattern (0.00) 0.67, and the strong variation in intensity of Ti II λ4064.35, which has the anomalous pattern (0.24, 0.71) 0.14, 0.62, 1.09, 1.57. Original dispersion of the spectrograms was 4.5 Å mm⁻¹.

PRESTON (see page 1059)

TABLE 1

JOURNAL OF OBSERVATIONS OF HD 126515

| Plate No.	J.D. (2400000+)	Phase	H_e (gauss)	H_s (λλ4086, 4385)	H_s (gauss) Fe, Cr	Ti	All Lines
Pb 3091.....	35884	0.31	+1310	12900	...	...	...
Pb 3147.....	35941	0.74	− 780	12400	...	...	...
Pb 5012.....	37003	0.91	−2100	15900	...	...	...
Pb 5018.....	37004	0.92	−1630	16600	16100	16200	16100
Pb 5022.....	37005	0.93	−2260	16500	16000	16900	16200
Pb 5108.....	37094	0.61	− 220	11100	...	...	...
Pb 5704.....	37360	0.66	− 580	11100	....	....	....
Pb 5829.....	37420	0.12	−1350	15700	16400	16400	16400
Pb 5887.....	37443	0.30	+1580	13300	...	...	...
Pb 5893.....	37444	0.31	+1630	12700	...	...	...
Pb 11070.....	40338	0.57	...	9800	...	...	...
Pb 11075.....	40339	0.58	...	10700	...	...	...
Pb 11095.....	40342	0.60	...	10600	...	...	...
Pb 11096.....	40342	0.60	...	10700	...	...	...
Ce 19742.....	40349	0.65	...	11200	...	...	...
Ce 19756.....	40365	0.78	...	13700	....	....	....
Ce 19798.....	40371	0.82	...	14700	14400	17800	15000
Pb 11155.....	40405	0.08	...	16500	16200	15700	16100
Pb 11218.....	40436	0.32	...	12200	...	...	...
Pb 11238.....	40458	0.49	...	10400	...	...	...
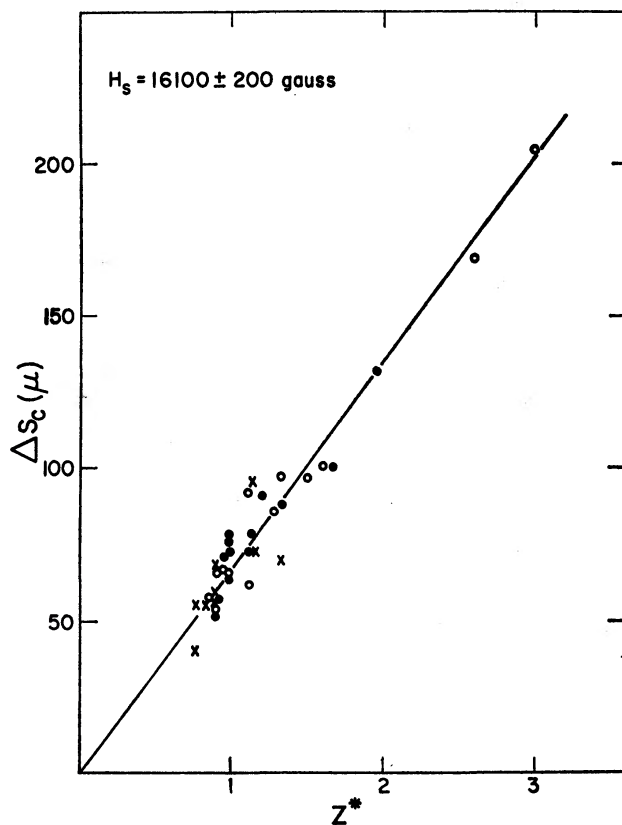
FIG. 2.—Correlation between component separation Δs_c and theoretical pattern width z^* for resolved Zeeman patterns on spectrogram Pb 11155 of HD 126515. *Open circles, filled circles,* and *crosses,* lines of Fe, Cr, and Ti, respectively. A mean surface field of 16100 gauss is obtained from the slope of the least-squares line through the origin.

1060

TABLE 2

LINES WITH RESOLVED ZEEMAN PATTERNS IN THE SPECTRUM OF HD 126515

λ	El (RMT)	Zeeman Pattern† (π) σ	z*	Δεc (microns)‡				
				Pb 5018	Pb 5022	Pb 5829	Ce 19798	Pb 11155
4022.36	Cr II (183)	(0.17, 0.51, 0.86) 0.34, 0.69, 1.03, 1.37, 1.71	0.89	58	63	...	58	53
4025.14	Ti II (11)	(0.08, 0.24, 0.40, 0.56) 0.59, 0.75, 0.91, 1.06, 1.22, 1.38, 1.54	0.76	54	57	55	49	40
4032.95	Fe II (126)	(0.31, 0.94, 1.57) −0.37, 0.26, 0.88, 1.51, 2.14	1.12	70	65	76	52	62
4076.87	Cr II (19)	(0.33, 1.00) 0.87, 1.53, 2.20	1.23	...	...	...	69	...
4086.14	Cr II (26)	(1.33) 1.33	1.33	87	88	90	79	88
4087.63	Cr II (19)	(1.67) 1.67	1.67	109	88	105	93	100
4113.24	Cr II (18)	(0.11, 0.34, 0.57) 1.03, 1.26, 1.48, 1.72, 1.94	0.99	62	77	81	67	78
4122.64	Fe II (28)	(0.29, 0.86, 1.43) 0.17, 0.74, 1.31, 1.89, 2.46	1.28	76	79	91	72	86
4151.00	Cr II (163)	(0.27, 0.80) 0.53, 1.07, 1.60	0.91	61	57	54	52	57
4174.09	Ti II (105)	(0.17, 0.51, 0.86) 0.34, 0.69, 1.03, 1.37, 1.71	0.89	58	...	66	54	58
4184.33	Ti II (21)	(0.20, 0.60) 0.60, 1.00, 1.40	0.78	...	59	56	65	56
4195.41	Cr II (161)	(0.20, 0.60, 1.00) 0.60, 1.00, 1.40, 1.80, 2.20	1.14	77	65	72	56	79
4202.03	Fe I (42)	(0.20, 0.40, 0.60, 0.80) 0.45, 0.65, 0.85, 1.05, 1.25, 1.45, 1.65, 1.85	0.91	63	61	65	60	66
4207.35	Cr II (26)	(0.11, 0.34, 0.57) 1.03, 1.26, 1.48, 1.72, 1.94	0.99	79	...	79	60	75
4210.35	Fe I (152)	(0.00) 3.00	3.00	200	...	...	222	204
4236.33	Cr II (17)	(0.14, 0.43, 0.71, 1.00) 0.71, 1.00, 1.28, 1.57, 1.85, 2.14, 2.43	1.20	82	90	86	97	91
4250.79	Fe I (42)	(0.33, 0.67, 1.00) 0.08, 0.42, 0.75, 1.08, 1.42, 1.75	0.89	52	52	49	52	54
4252.62	Cr II (31)	(0.17, 0.51, 0.86) 0.51, 0.86, 1.20, 1.54, 1.89	0.98	67	68	67	70	64
4260.48	Fe I (152)	(0.00) 1.60	1.60	115	114	123	115	101
4273.32	Fe II (27)	(0.87) 0.87, 260	0.87 / 2.60	... / ...	63 / 169	... / ...	58 / 172	58 / 169
4274.80	Cr I (1)	(0.08, 0.17, 0.25) 1.75, 1.83, 1.92, 2.00, 2.08, 2.17	1.96	134	146	140	134	132
4303.17	Fe II (27)	(0.27, 0.80) 0.93, 1.47, 2.00	1.11	86	86	88	82	92
4312.86	Ti II (41)	(0.11, 0.34, 0.57) 1.03, 1.26, 1.48, 1.72, 1.94	0.99	67	...	59	59	...
4314.98	Ti II (41)	(1.33) 1.33	1.33	77	76	82	73	70
4369.40	Fe II (28)	(1.13) 0.73, 1.53	...	68	74	78	79	78
4385.38	Fe II (27)	(1.33) 1.33	1.33	92	94	95	91	97
4404.75	Fe I (41)	(0.00, 0.07, 0.13, 0.20) 0.95, 1.02, 1.08, 1.15, 1.22, 1.28, 1.35	1.25	...	...	...	65	...
4416.82	Fe II (27)	(0.73) 0.47, 1.93	...	...	...	...	...	...
4421.95	Ti II (93)	(0.27, 0.80) 0.53, 1.07, 1.60	0.91	60	72	64	65	68
4441.73	Ti II (40)	(0.20, 0.60, 1.00) 0.60, 1.00, 1.40, 1.80, 2.20	1.14	82	85	75	101	95
4450.49	Ti II (19)	(0.17, 0.51, 0.86) 0.34, 0.69, 1.03, 1.37, 1.71	0.89	59	59	49	60	57
4520.22	Fe II (37)	(0.05, 0.14, 0.24, 0.33) 1.00, 1.09, 1.19, 1.28, 1.38, 1.48, 1.57, 1.67	1.50	103	97	...	94	97
4529.46	Ti II (82)	(0.10, 0.30, 0.50, 0.71, 0.91) 0.20, 0.40, 0.61, 1.01, 1.21, 1.41, 1.62, 1.82	0.88	55	61	62	71	57
4539.62	Cr II (39)	(0.26, 0.77, 1.29) 0.60, 1.12, 1.63, 2.14	1.12	71	67	69	70	73
4544.01	Ti II (60)	(0.20, 0.60, 1.00) 0.60, 1.00, 1.40, 1.80, 2.20	1.14	92	86	...	87	73
4555.02	Cr II (44)	(0.10, 0.29, 0.48, 0.67) 0.76, 0.95, 1.14, 1.33, 1.52, 1.72, 1.90	0.95	64	71	69	57	71
4576.33	Fe II (38)	(0.17, 0.51, 0.86) 0.51, 0.86, 1.20, 1.54, 1.89	0.98	66	66	70	64	66
4592.09	Cr II (44)	(0.17, 0.51, 0.86) 0.51, 0.86, 1.20, 1.54, 1.89	0.98	59	67	65	62	72
4620.51	Fe II (38)	(0.10, 0.29, 0.48, 0.67) 0.76, 0.95, 1.14, 1.33, 1.52, 1.72, 1.90	0.95	69	...	...	66	67

†The pattern notation is that of Kiess and Meggers (1928). Most intense components are indicated by boldface.

‡The dispersions for the Pb and Ce spectrograms are 4.53 and 4.35 Å mm⁻¹, respectively.

(4) below. We shall refer to the quantity H_s derived from measures of resolved Zeeman patterns as the *mean surface field*. This description of H_s arises as follows. To each area element dA on the stellar disk there corresponds a local field of magnitude $|H|$ that produces line components with a separation

$$\Delta\lambda = 9.33 \times 10^{-13} \lambda^2 \, |H| z^* \,, \tag{1}$$

where λ is in angstroms, H is in gauss, and $z^* = z$ for the σ-components of triplets or z' for the π-σ complexes of doublets. In the unpolarized, integrated light of the star, the separation of the centroids of the observed components is an average over the disk of the local separation $\Delta\lambda$ weighted by the local surface brightness, I,

$$\langle\Delta\lambda\rangle = 9.33 \times 10^{-13}\lambda^2 z \frac{\int |H| I dA}{\int I dA} \,. \tag{2}$$

If we write

$$H_s = \frac{\int |H| I dA}{\int I dA} \,, \tag{3}$$

we recover Babcock's (1958) familiar least-squares expression, but for H_s instead of H_e,

$$H_s = 52.7 F \frac{\Sigma \Delta s_c}{\Sigma z^*} \,. \tag{4}$$

As will be evident in what follows, the variation of H_s provides valuable new information about a magnetic star.

II. THE VARIATIONS IN H_s AND H_e

On occasion, the mean surface field of HD 126515 becomes so small that most of the lines in Table 2 are not resolved. However, the two doublets Cr II $\lambda4086.14$ and Fe II $\lambda4385.38$, with the simple Zeeman pattern (1.33) 1.33, are clearly resolved on *all* spectrograms of HD 126515. Therefore, H_s was determined for each spectrogram from measures of these two lines. The results are given in column (5) of Table 1. A plot of these results versus Julian Date gave indication that H_s varies regularly with a period near 130 days, and the best representation was found to be given by

$$\text{J.D. } (H_s \text{ maximum}) = 2437015.0 + 130\overset{d}{.}0 \, E \,, \tag{5}$$

where E is the number of elapsed cycles. The variation in H_s that results from the use of phases calculated by means of equation (5) is illustrated in Figure 3. The mean surface field oscillates in an approximately sinusoidal manner between 10 and 17 kilogauss.

If HD 126515 is a rigid rotator, that is, if the observed variation of H_s is an aspect effect produced by the rotation of a static surface field, then the surface field cannot be that of a centered dipole because the observed ratio H_s (max)/H_s (min) = 1.7 significantly exceeds the maximum possible ratio (=1.25) for a centered dipole (Preston 1969b). The nature of the departure from a centered-dipole field is indicated by the variation of the effective field H_e, also shown in Figure 3. The latter is obtained from Miss Sylvia Burd's measurements of Babcock's series of spectrograms. The effective field varies between -2 and $+2$ kilogauss with a single wave in the 130-day period. Comparison of the variations in H_s and H_e shows clearly that when H_e is negative, H_s is large, and when H_e is positive, H_s is small. This behavior rules out a centered-dipole field because for dipole geometry H_s must exhibit a double wave during a single cycle of the H_e variation, if H_e (min) $\approx -H_e$ (max). Instead, the observed H_s variation indicates that the magnetic flux is not symmetric with respect to a magnetic equator, but rather is concentrated in that hemisphere which gives rise to a negative effective field.

III. A DECENTERED-DIPOLE MODEL

The simplest axisymmetric divergence-free surface field that can produce ranges in H_s and H_e similar to those of HD 126515 is that of a magnetic dipole displaced from the center of the star in the direction of its moment. Such a model has been proposed recently by Landstreet (1970) to represent the H_e variation of 53 Cam. If the displacement in, say, the z-direction in units of the stellar radius is a, then the ratio of the fields at $z = +1$ and $z = -1$ is $[(1 + a)/(1 - a)]^3$; a modest value of a can produce the observed range of H_s. It remains to determine whether such a decentered dipole can be inclined to the rotation axis at some angle β so that, if the star is viewed at some inclination i, the observed variations of both H_s and H_e can be produced simultaneously.

Consider a dipole located at $(0, 0, a)$ in an (x, y, z) system of coordinates with origin at the center of a star of unit radius. Let the dipole moment lie in the positive z-direction.
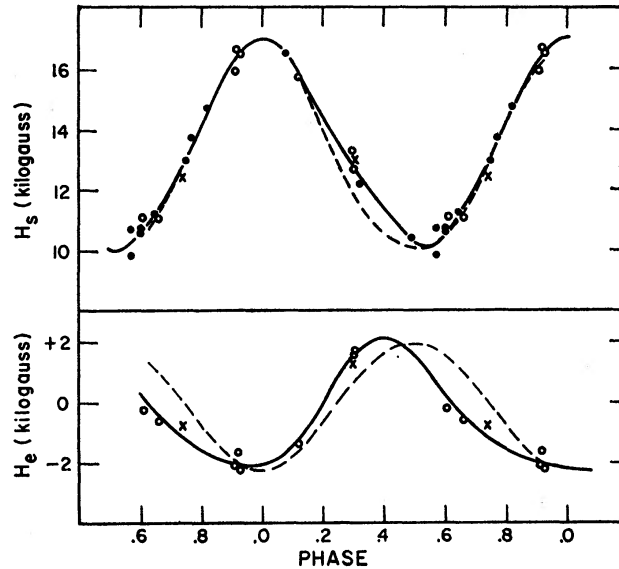

Fig. 3.—Variation of the mean surface field H_s and the effective field H_e with phase in the 130^d0 cycle of HD 126515. *Crosses, open circles,* and *filled circles,* observations made in 1957, 1960, and 1969, respectively. *Solid curves,* freehand representations of the variations. *Dashed curves,* variations for the decentered-dipole model discussed in § III of the text.

If we measure the surface field in units of the field at $z = +1$, we obtain the rectangular components

$$h_x = \frac{3(1 - a)^3}{2} \frac{x(z - a)}{D^5}, \qquad h_y = \frac{3(1 - a)^3}{2} \frac{y(z - a)}{D^5}$$

and

$$h_z = \frac{(1 - a)^3}{2} \frac{[3(z - a)^2 - D^2]}{D^5}, \qquad (6)$$

with

$$h = \frac{(1 - a)^3}{2} \frac{[3(z - a)^2 + D^2]^{1/2}}{D^4}, \qquad (7)$$

where

$$D^2 = 1 + a^2 - 2az. \qquad (8)$$

Let an observer view the star from the ζ-direction of a (ξ, η, ζ) system of coordinates, and let the ζ-axis lie in the (x, z) plane, inclined at angle α to the z-axis. The two coordinate systems are related by the transformations

$$x = \zeta \sin \alpha + \xi \cos \alpha, \qquad y = \eta, \qquad z = \zeta \cos \alpha - \xi \sin \alpha. \qquad (9)$$

The component of the field in the ζ-direction at any point on the disk is

$$h_\zeta = h_z \cos a + h_x \sin a . \tag{10}$$

Therefore, if we employ the usual limb-darkening law

$$I = 1 - u + u\zeta , \tag{11}$$

where

$$\zeta^2 = 1 - \xi^2 - \eta^2 , \tag{12}$$

TABLE 3

VALUES OF h_e AS A FUNCTION OF COS a AND THE DECENTERING PARAMETER a

	cos a						
a	1.000	0.866	0.500	0.000	−0.500	−0.866	−1.000
0.0	0.3141	0.2720	0.1570	0.0000	−0.1570	−0.2720	−0.3141
0.05	0.2754	0.2370	0.1338	−0.0035	−0.1358	−0.2290	−0.2623
0.10	0.2383	0.2044	0.1132	−0.0060	−0.1167	−0.1909	−0.2164
0.20	0.1713	0.1467	0.0794	−0.0085	−0.0841	−0.1280	−0.1415
0.40	0.0717	0.0624	0.0343	−0.0076	−0.0378	−0.0479	−0.0498
0.60	0.0191	0.0171	0.0105	−0.0037	−0.0119	−0.0121	−0.0119
0.80	0.0009	0.0011	0.0010	−0.0008	−0.0015	−0.0012	−0.0011

TABLE 4

VALUES OF h_s AS A FUNCTION OF COS a AND THE DECENTERING PARAMETER a

	cos a						
a	1.000	0.866	0.500	0.000	−0.500	−0.866	−1.000
0.0	0.7671	0.7253	0.6441	0.6044	0.6441	0.7253	0.7671
0.05	0.7244	0.6779	0.5826	0.5184	0.5242	0.5715	0.5981
0.10	0.6796	0.6297	0.5235	0.4413	0.4236	0.4473	0.4632
0.20	0.5850	0.5318	0.4134	0.3116	0.2694	0.2673	0.2709
0.40	0.3860	0.3388	0.2301	0.1344	0.0935	0.0827	0.0803
0.60	0.1977	0.1681	0.1000	0.0415	0.0227	0.0181	0.0170
0.80	0.0552	0.0456	0.0239	0.0055	0.0023	0.0017	0.0015

we obtain the normalized effective field

$$h_e \equiv \langle h_\zeta \rangle = \frac{3(1 - a)^3}{\pi(3 - u)}$$

$$\times \int_{-1}^{+1} d\xi \int_0^{\sqrt{1-\xi^2}} \left[\frac{1}{D^5} \{ [3(z - a)^2 - D^2] \cos a + 3x(z - a) \sin a \} \right] I(\xi, \eta) d\eta \tag{13}$$

and the normalized mean surface field

$$h_s \equiv \langle h \rangle = \frac{3(1 - a)^3}{\pi(3 - u)} \int_{-1}^{+1} d\xi \int_0^{\sqrt{1-\xi^2}} \frac{[3(z - a)^2 + D^2]^{1/2}}{D^4} I(\xi, \eta) d\eta . \tag{14}$$

In equations (13) and (14), the quantities x, z, and D can be expressed as functions of ξ and η by means of equations (7)–(10) and (12).

Numerical values of h_e and h_s and their ratio h_e/h_s are given in Tables 3, 4, and 5 as

functions of cos a for seven values of the decentering parameter a. The calculations were made on an IBM 360-75 computer with the aid of a program written by Mr. Donn Hall of the California Institute of Technology. The results, displayed in Figures 4, 5, and 6, are used in the model-fitting procedure as follows. The observed maximum and minimum values of h_e/h_s are, from Figure 3, $+\frac{2}{17} = +0.118$ and $-\frac{2}{10} = -0.200$ (we reverse the signs of the observed ratios because our calculations were made for a dipole displaced in the direction of its moment, while for HD 126515 the opposite case must obtain). The extrema plotted as horizontal lines in Figure 6 determine upper and lower limits cos a_u and cos a_l for each value of a. To each pair of limits there correspond values of h_e (cos $a_l)/h_e$ (cos a_u) and h_s (cos a_l/h_s (cos a_u), as indicated in Figures 5 and 6. If we enter plots of these ratios versus a with the observed ratios -1.0 and $+1.7$ (again, with signs reversed), we obtain two independent estimates of a, 0.350 and 0.366, respectively; we adopt $a = 0.36$. Interpolation among the cosine limits for the various a-values taken from Figure 6 then gives (see Stibbs 1950 or Preston 1967b)

$$\cos a_l = \cos (\beta - i) = +0.38 , \quad \cos a_u = \cos (\beta + i) = -0.22 , \quad (15)$$

so that β and i have the values 17° and 85° or 85° and 17°, respectively. If $H_{z=+1} = -74$ kilogauss, then the above values of a, β, and i give the best representations of the H_s

TABLE 5

VALUES OF h_e/h_s AS A FUNCTION OF COS a AND THE DECENTERING PARAMETER a

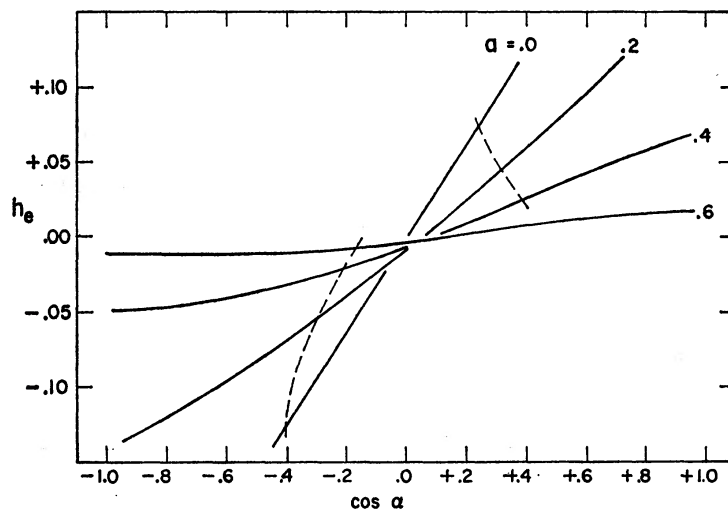| a	COS a						
	1.000	0.866	0.500	0.000	−0.500	−0.866	−1.000
0.0	0.4095	0.3751	0.2438	0.0000	−0.2438	−0.3751	−0.4095
0.05	0.3801	0.3497	0.2296	−0.0068	−0.2591	−0.4008	−0.4386
0.10	0.3507	0.3246	0.2164	−0.0136	−0.2755	−0.4267	−0.4672
0.20	0.2927	0.2759	0.1921	−0.0274	−0.3122	−0.4788	−0.5223
0.40	0.1858	0.1844	0.1493	−0.0565	−0.4047	−0.5801	−0.6202
0.60	0.0966	0.1020	0.1052	−0.0901	−0.5246	−0.6701	−0.6992
0.80	0.0176	0.0242	0.0440	−0.1479	−0.6551	−0.7424	−0.7604

FIG. 4.—Variation of h_e, the effective field in units of the surface field at $z = +1$, with cos a for four values of the decentering parameter a. Dashed lines connect the limits on cos a for each value of a that are inferred from the observed maximum and minimum values of the ratio h_e/h_s in Fig. 6.

and H_e variations of HD 126515 that are possible with a decentered-dipole model. The model variations of H_s and H_e are indicated as dashed curves in Figure 3. The model successfully predicts the ranges of H_s and H_e and gives a fair representation of the H_s variation. However, it cannot predict the observed phase shift of ~ 0.1 cycle between the H_e and H_s variations. This shift indicates a departure from axial symmetry.

IV. SPECTRUM VARIABILITY

a) Line-Strength Measurements

Well-marked spectrum variations occur during the magnetic cycle of HD 126515. The most conspicuous variations are those of Ti II—for example, $\lambda4064.35$ in Figure 1—
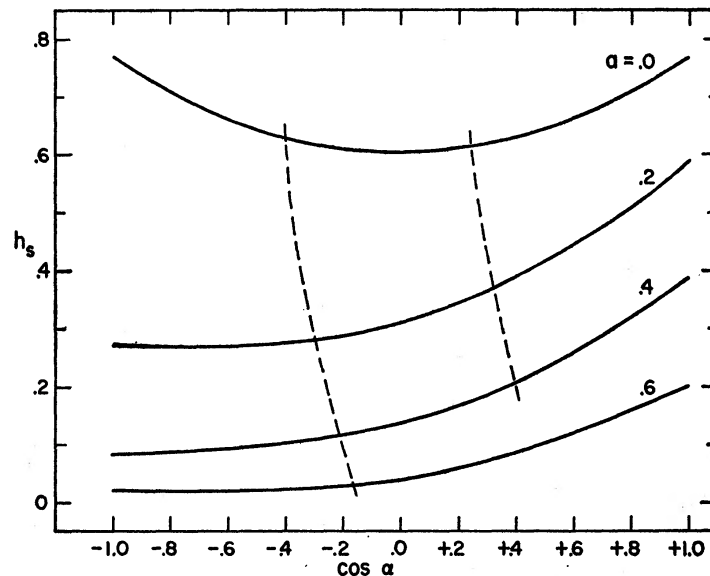
FIG. 5.—Variation of h_s, the mean surface field, in units of the surface field at $z = +1$, with cos a for four values of the decentering parameter a. Dashed lines connect the limits on cos a for each value of a that are inferred from the observed maximum and minimum values of the ratio h_e/h_s in Fig. 6.
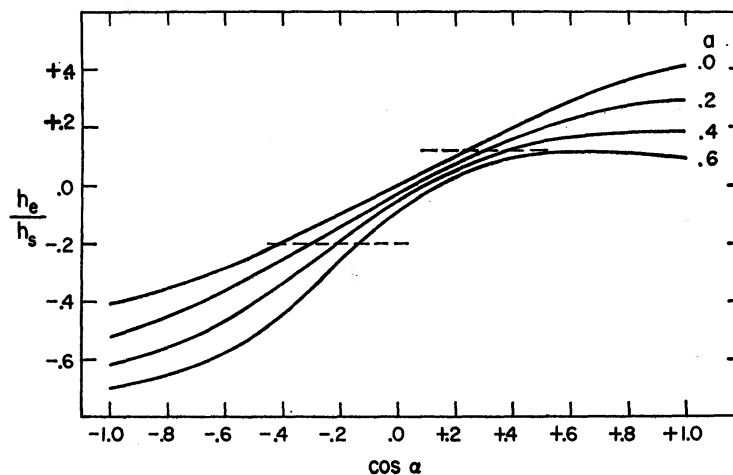
FIG. 6.—Variation of the ratio h_e/h_s with cos a for four values of the decentering parameter a. Observed maximum and minimum values of h_e/h_s are indicated by horizontal dashed lines. Intersections of these lines with computed curves give upper and lower limits on cos a for each value of a.

but variations are also apparent for lines of Si, Cr, Fe, Sr, and Eu, and it seems likely that *all* lines participate in this phenomenon to some extent. In order to delineate these variations quantitatively, eleven lines of Ti II, twelve lines of Fe I and Fe II, and sixteen lines of Cr I and Cr II were measured on microphotometer tracings of the sixteen best spectrograms. The Si II lines $\lambda\lambda 4128$ and 4130 and the Eu II lines $\lambda\lambda 4205$ and 4435 were also measured. For each line a pseudo-equivalent width dw, the product of central depth and width at half-depth, was formed. More precise measurements were not attempted for two reasons: (1) more than half of the spectrograms are uncalibrated for photometry, and as a consequence a single mean calibration curve was used for all spectrograms; and (2) a number of profiles show incipient π-σ resolution near the phase of maximum H_s but not at other phases. Precise measures of the true equivalent widths of such blends would be arduous and probably not justified in view of the approximate calibration.
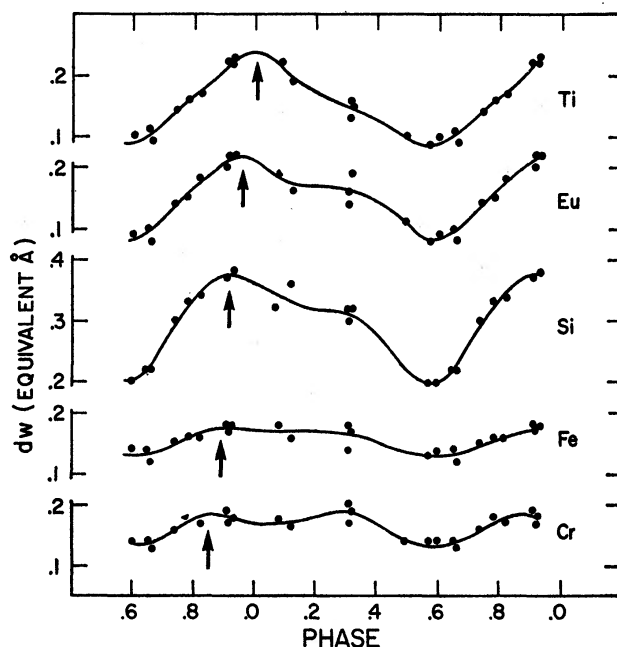
FIG. 7.—Variation in line strength dw with phase for five elements in the spectrum of HD 126515. The apparent progression in the phase of maximum intensity Ti → Cr is discussed in the text. Note single wave for Ti and double wave for Cr.

The results on spectrum variation for five elements are summarized in Figure 7. Comparison of Figures 3 and 7 shows immediately that line strength and mean surface field strength are correlated. All lines are weakest near the phase of minimum H_s, and for Ti, Eu, and Si, at least, maximum line strength occurs *near* the phase of maximum H_s. However, intercomparison of the curves for the various elements indicates that there are real differences in the forms of the variations. If limited quality and quantity of the data are borne in mind, it is possible to arrange the elements in a sequence Ti-Eu-Si-Fe-Cr in which a primary maximum shifts from phase 0.0 for Ti to earlier phases by a total of ~0.15 cycle, and diminishes in height relative to a secondary maximum at phase 0.3 (largely imaginary in the case of Ti) that becomes relatively more conspicuous at the end of the sequence. In the case of Cr, the maximum at phase 0.3 is probably the primary maximum. Unlike any spectrum variable studied heretofore, e.g., α^2 CVn, 73 Dra, or HD 125248, the Cr and Eu lines of HD 126515 do not vary in antiphase. Rather, they share a common phase of minimum strength but differ with respect to the phase of primary maximum.

b) Magnetic Intensification of Spectral Lines

Magnetic intensification of a saturated spectral line will occur if the Zeeman splitting exceeds the Doppler width. The effects that can be expected have been discussed by Babcock (1949), Unno (1956), and in greatest detail by Boyarchuk, Efimov, and Stepanov (1960). Because many spectral lines of HD 126515, particularly those of Ti II, wax and wane in phase with the mean surface field, one may inquire as to whether magnetic intensification is responsible for any part of the observed ranges in line strength. The apparent correlation between line strength and H_s does not by itself constitute a prima facie case because the surface concentration of heavy elements may be correlated with field strength. Indeed, the large range of Ti II $\lambda 4064$ in Figure 1 cannot be explained solely by a process that depends on saturation effects; the line is vanishingly weak at phase 0.57.

A test for the occurrence of magnetic-intensification effects in HD 126515 was made as follows. Curves similar to those in Figure 7 were constructed for *the individual lines* of Ti II. For each curve, two quantities were formed: the range Δ_{05}, taken as the difference between line strengths at phases 0.0 (H_s maximum) and 0.5 (H_s minimum), and the time-averaged line strength $\langle dw \rangle$. The fractional ranges $\Delta_{05}/\langle dw \rangle$ were then plotted versus z-values, which characterize the Zeeman splitting; there is no correlation. Since examination of Figure 1 shows that Zeeman splitting $\Delta\lambda_z$ clearly exceed Doppler widths $\Delta\lambda_D$ at some phases, this result can only mean that *at all phases* the lines are subject to an approximately constant magnetic intensification due to π-σ resolution. For this to be true we must have

$$\frac{\Delta\lambda_z}{\Delta\lambda_D} = 6 \times 10^{-4} \frac{Hz}{v} \gtrsim 1 . \tag{16}$$

Since $H_s \geq 10^4$ gauss at all phases and the Doppler parameter v probably is not in excess of 3 km sec^{-1} (Preston 1967a; Preston and Cathey 1968), we find indeed that for $z = 1$ the ratio is always greater than 2 over a significant portion of the stellar disk.

A second kind of Zeeman intensification can occur if the interval δ between adjacent subcomponents of the π and σ groups in anomalous patterns exceeds the Doppler width. If we replace z by δ in equation (16), the condition for this type of intensification becomes, approximately,

$$H \gtrsim 1.7 \times 10^3 \, v/\delta . \tag{17}$$

For $v = 3$ km sec^{-1} and $\delta = 0.3$ (a typical value), we must have $H \gtrsim 1.7 \times 10^4$ gauss, a value equal to H_s (maximum). Therefore, for those portions of the disk where local fields exceed the mean (H_s) and for transitions for which $\delta > 0.3$ this kind of intensification should be present, and it should vary with phase. It should increase with δ, with the number of subcomponents n, and therefore with $n\delta$. Marginal evidence for a correlation of this kind for Ti II is shown in Figure 8. The scatter can be due to a number of factors in addition to errors of spectrophotometry: For some transitions the π and σ groups overlap, while for others they do not; for some patterns the weakest subcomponents may be saturated and hence subject to intensification, while for others they may not be saturated; for some patterns the most intense σ and/or π components are the inner ones, while in other cases they are the outer ones. All these circumstances will affect the degree of intensification, and it is not possible to disentangle all of the effects from measurement errors and from each other with a limited number of lines. The fact that similar correlations could not be found for Cr and Fe can be interpreted in one of several ways: (1) the phenomenon does not exist and the correlation for Ti is accidental; (2) the correlation for Ti is real but errors and/or an unfortunate selection of Cr and Fe lines masks the correlations for these elements; or (3) the phenomenon occurs for Ti but not for Cr and Fe because the Ti abundance is relatively high in large-field regions of

the stellar surface while the Cr and Fe abundances are relatively low. This last alterna-
tive may seem implausible, but from the point of view of the rigid-rotator model it
would follow from a straightforward interpretation of the double wave in the Cr varia-
tion relative to the single wave for Ti in Figure 7. The true state of affairs is likely to be
more complicated than we have imagined. For the few plates near H_s maximum from
which fields can be derived separately from Ti and from Cr and Fe (see Table 1), it
appears that H_s (Ti) $>$ H_s (Cr-Fe) prior to phase zero and H_s (Ti) $\lesssim H_s$ (Cr-Fe) just
after phase zero. Unfortunately, the Ti doublets are not numerous and their z-values
are not outstandingly large. Consequently, the reality of these effects is hardly certain.
Clearly, more accurate measures of the variations in line intensity and magnetic field
of HD 126515 would be highly desirable, as they may provide rewarding results about
an interesting spectroscopic phenomenon and perhaps about the distribution of elements
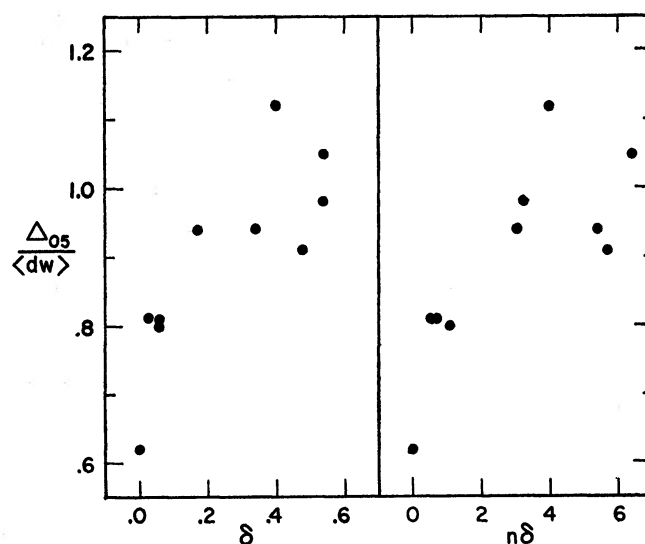on the surface of a magnetic star as well.

FIG. 8.—Evidence for variable Zeeman intensification of Ti II lines in the spectrum of HD 126515.
The fractional range in line strength $\Delta_{05}/\langle dw \rangle$ appears to increase with the interval δ between adjacent
Zeeman subcomponents and with the product of δ and n, the number of such subcomponents in the
pattern.

V. DISCUSSION

Arguments in favor of the rigid-rotator model for magnetic stars have been advanced
first by Stibbs (1950) and Deutsch (1952, 1956), later by Steinitz (1967), and most
recently by the writer (Preston 1970), and they need not be repeated here. If these
arguments are accepted, then the results for HD 126515 provide new insight into the
nature of the surface of a magnetic star:

1. The H_s and H_e variations provide direct evidence that the surface field of a mag-
netic star can exhibit a strong hemispherical asymmetry even though the effective (net
longitudinal) field oscillates about zero between nearly symmetrical limits. Analysis of
the observations in terms of a simple decentered-dipole model indicates that it is not
difficult to find surface-field distributions that possess this unanticipated property. Simi-
lar contemporary conclusions have been reached for β CrB (Wolff and Wolff 1970). These
results, in turn, lend credence to the asymmetrical field distributions for HD 125248
(Deutsch 1958) and α^2 CVn (Pyper 1969) that were inferred from harmonic analysis of
the variations in H_e, radial velocity, and line intensity of those stars.

2. Babcock (1958) noted that the lines of 53 Cam are broader at the negative ex-
tremum of the H_e variation than at the positive extremum. A similar result was obtained

for β CrB by Preston and Sturch (1967), and the writer (Preston 1967c) noted that this is a common characteristic of periodic magnetic stars. More recently, resolved Zeeman patterns were discovered in 53 Cam when H_e was negative (Preston 1969a), and subsequent examination of other spectrograms of this star by the writer indicates that these patterns are invariably resolved when $H_e < 0$ and unresolved when $H_e > 0$. The hemispherical asymmetry required by HD 126515 explains these results on line width in a natural way.

3. The fact that the line strengths for Si, Ti, Sr, and Eu vary in phase with H_s in HD 126515 strongly suggests that these elements tend to be concentrated in regions of intense magnetic field. It has long been recognized that line-intensity maxima coincide in phase with an extremum of the effective field for numerous periodic magnetic stars. The present results indicate an important physical difference between regions of opposite polarity that could not be inferred from the H_e data alone.

4. Finally, the equality of photometric and magnetic periods has been used as an argument against the rotator model because there is no physical reason why surface brightness should depend on magnetic polarity. However, for HD 126515 we now know that the mean surface field varies by a factor of 1.7. A decentered-dipole model that produces this factor requires a decentering parameter of $a = 0.36$, for which the ratio of negative to positive polar-field strengths is $[(1 + a)/(1 - a)]^3 \sim 10$, and hence the ratio of polar magnetic energy densities is ~ 100. Thus it is conceivable, though not yet demonstrated, that variations in surface brightness are somehow linked to strong surface variations of the magnetic-energy density.

To summarize, the observed H_s and H_e variations of HD 126515 require that the star possess a hemispherically asymmetric field distribution not greatly unlike that of a decentered dipole. This type of field distribution is consistent with field distributions inferred for other stars by indirect methods, it explains an extensive body of data on variable line widths in periodic magnetic stars, and it holds promise of providing reasons for the nonuniform surface concentration of heavy elements and the aspect-dependent luminosities that are required of magnetic stars if they are rigid rotators.

REFERENCES

Babcock, H. W. 1949, *Ap. J.*, **110**, 126.
———. 1958, *Ap. J. Suppl.*, **3** (No. 31), 141.
Boyarchuk, A. A., Efimov, Yu. S., and Stepanov, V. E. 1960, *Soviet Astr.—AJ*, **37**, 812.
Deutsch, A. J. 1952, *Trans. I.A.U.*, ed. P. Th. Oosterhoff (Cambridge: Cambridge University Press), **8**, 801.
———. 1956, *Pub. A.S.P.*, **68**, 92.
———. 1958, *I.A.U. Symp. No. 6*, ed. B. Lehnert (Amsterdam: North-Holland Publishing Co.), p. 209.
Kiess, C., and Meggers, W. 1928, *J. Res. N.B.S.*, **1**, 641.
Landstreet, J. D. 1970, *Ap. J.*, **159**, 1001.
Preston, G. W. 1967a, *Ap. J.*, **147**, 804.
———. 1967b, *ibid.*, **150**, 547.
———. 1967c, in *The Magnetic and Related Stars*, ed. R. Cameron (Baltimore: Mono Book Corp.), p. 3.
———. 1969a, *Ap. J.*, **157**, 247.
———. 1969b, *ibid.*, **158**, 1081.
———. 1970, in *I.A.U. Symp. on Stellar Rotation*, ed. A. Slettebak (Dordrecht: D. Reidel Publishing Co.) (in press).
Preston, G. W., and Cathey, L. R. 1968, *Ap. J.*, **152**, 1113.
Preston, G. W., and Sturch, C. 1967, in *The Magnetic and Related Stars*, ed. R. Cameron (Baltimore: Mono Book Corp.), p. 111.
Pyper, D. M. 1969, *Ap. J. Suppl.*, **18** (No. 164), 347.
Steinitz, R. 1967, in *The Magnetic and Related Stars*, ed. R. Cameron (Baltimore: Mono Book Corp.), p. 83.
Stibbs, D. W. N. 1950, *M.N.R.A.S.*, **110**, 395.
Unno, W. 1956, *Pub. Astr. Soc. Japan*, **8**, 108.
Wolff, S. C., and Wolff, R. J. 1970, *Ap. J.*, **160**, 1049.